Dalton Transactions

PAPER

View Article Online
View Journal | View Issue

Cite this: *Dalton Trans.*, 2015, **44**, 10368

Energy transfer and unusual decay behaviour of $BaCa_2Si_3O_9:Eu^{2+},Mn^{2+}$ phosphor†

Matthias Müller and Thomas Jüstel*

Received 9th February 2015,
Accepted 22nd April 2015

DOI: 10.1039/c5dt00591d

www.rsc.org/dalton

In this work the photoluminescence (PL) of $BaCa_2Si_3O_9:Eu^{2+},Mn^{2+}$ and the energy transfer (ET) between Eu^{2+} and Mn^{2+} were examined. A series of powder samples with various Mn^{2+} concentrations were prepared by high temperature solid state route. Phase purity was investigated using X-ray powder diffractometry. Emission and excitation spectra as well as diffuse reflectance spectra were recorded to elucidate the PL properties of co-doped $BaCa_2Si_3O_9:Eu^{2+},Mn^{2+}$. Furthermore, fluorescence lifetime measurements were performed. PL and lifetime measurements were carried out from 100 to 800 K and 100 to 500 K, respectively. Moreover, external quantum efficiencies were determined and colour points were calculated. It turned out that ET from Eu^{2+} to Mn^{2+} is of a resonant type and occurs *via* dipole–quadrupole interactions. Temperature dependent PL measurements indicate high temperature stability of emission intensity in $BaCa_2Si_3O_9:Eu^{2+},Mn^{2+}$. Finally, it was found that fluorescence lifetimes of Eu^{2+} $BaCa_2Si_3O_9$ show an unusual increase with increasing temperature.

1. Introduction

Even though the invention of bright blue light emitting diodes (LEDs) by Nakamura *et al.* nearly dates back a quarter of a century, LEDs still have a vast impact on advances in lighting technology.[1] Meanwhile, LEDs have replaced more and more conventional light sources such as incandescent and discharge lamps. This is because of the fact that LEDs provide many benefits compared to thermal and gas discharge light sources, such as longer lifetimes, higher wall plug efficiency and higher colour rendering.[2] Nowadays, most of the commercially available white light emitting LEDs comprise a blue emitting (In,Ga)N chip pumping a green-yellow emitting phosphor, *e.g.* $(Y,Gd)_3Al_5O_{12}:Ce^{3+}$. This setup provides a high luminous efficacy due to emission in the green spectral range. Unfortunately, these lamps suffer from high colour temperature and low colour rendering index due to the lack of emission in the red spectral range.[3] Therefore, these light sources are unpopular for domestic lighting. To overcome these drawbacks, one approach is to use a phosphor blend comprising a blue, green, and red phosphor, which is excited by an ultraviolet emitting LED. Using this concept, cold and warm white emitting LEDs with excellent colour points can be realized.[4] However, these packages undergo a loss in blue emission due to re-absorption by the green and red phosphors. For this reason, many research groups are developing single phase white emitting phosphors to convert UV radiation into white light.[5]

One approach to realize a white emitting phosphor is to use the ion couple Eu^{2+} and Mn^{2+}.[6] The broad emission bands in the blue and red spectral range of Eu^{2+} and Mn^{2+} in many host structures complement each other to white light due to additive colour mixing. Furthermore, Eu^{2+} usually exhibits a broad excitation band in the UV range due to the spin and parity allowed $[Xe]4f^7$–$[Xe]4f^65d^1$ interconfigurational electric-dipole transition. Therefore, Eu^{2+} is well appropriated for pumping by UV LEDs. In addition the blue emission band of Eu^{2+} is also suitable for sensitizing the spin and parity forbidden $[Ar]3d^5$–$[Ar]3d^5$ excitation transitions of Mn^{2+} *via* energy transfer (ET). To investigate the photoluminescence (PL) properties as well as the ET from Eu^{2+} to Mn^{2+}, a series of co-doped $BaCa_2Si_3O_9:Eu^{2+},Mn^{2+}$ samples with various Mn^{2+} concentrations were synthesized. $BaCa_2Si_3O_9$ was described for the first time in the work of Eskola in 1922.[7] Later on, in 1965 Alfors *et al.* investigated the mineral walstromite.[8] Based on their results on optical properties and X-ray powder diffraction data they stated that $BaCa_2Si_3O_9$ is identical to walstromite. Glasser *et al.* reported on the crystal structure of synthetic $BaCa_2Si_3O_9$ using photographic X-ray diffraction data in 1968.[9] The crystal structure derived from a single crystal analysis of $BaCa_2Si_3O_9$ was firstly published by Barkley *et al.* in 2011.[10] Shortly afterwards, Yao *et al.* presented the first report on the

Department of Chemical Engineering, Münster University of Applied Sciences, Stegerwaldstrasse 39, 48565 Steinfurt, Germany. E-mail: tj@fh-muenster.de

†Electronic supplementary information (ESI) available: PLD curves of $Ba_{0.99}Eu_{0.01}Ca_2Si_3O_9$ monitored at 415 and 495 nm, PL integrals of Eu^{2+} and Mn^{2+} in dependence of temperature, PL spectra of $Ba_{0.99}Eu_{0.01}Ca_2Si_3O_9$ from 100 to 800 K and PL integral in dependence of temperature, PLD curve of $Ba_{0.99}Eu_{0.01}Ca_2Si_3O_9$ monitored at λ_{em} = 700 nm and T = 77 K, simulated white emission spectrum. See DOI: 10.1039/c5dt00591d

blue emission of Eu^{2+} doped $BaCa_2Si_3O_9$.[11] Moreover, Gaft *et al.* published an article concerning the luminescence of natural walstromite in 2013.[12]

$BaCa_2Si_3O_9$ crystallizes triclinically in the space group $P\bar{1}$. The structure of triclinic $BaCa_2Si_3O_9$ is built up of layers consisting of alternating Si_3O_9 rings. Between these layers Ba and Ca atoms are incorporated. $BaCa_2Si_3O_9$ comprises two non-equivalent Ca sites, namely Ca1 and Ca2. The Ca1 site is coordinated by 8 oxygen atoms with a mean distance of 2.545 Å. The Ca2 site is surrounded by 6 oxygen atoms with an average bond length of 2.370 Å. The Ba atoms are 8-fold coordinated with an average distance of 2.841 Å. The ionic radii of Ca for 8 and 6-fold coordination are 1.12 and 0.96 Å. Ba^{2+} in 8-fold coordination has an ionic radius of 1.42 Å. The ionic radii of Mn^{2+} and Eu^{2+} for 8 and 6-fold coordination are 0.96 and 0.83 as well as 1.25 and 1.17 Å, respectively.[13] Based on the ionic radii, it can be assumed that the Mn^{2+} ions tend to occupy the Ca sites whereas the Eu^{2+} ions tend to occupy the Ba^{2+} sites as well as the 8-fold coordinated Ca^{2+} sites.

2. Experimental

Preparation

$Ba_{0.99}Eu_{0.01}(Ca_{1-x}Mn_x)_2Si_3O_9$ samples were synthesized *via* conventional high temperature solid state reaction. High purity starting materials $BaCO_3$ (Alfa Aesar, 99.8%), $CaCO_3$ (Merck KGaA, Reag. Ph. Eur.), SiO_2 (Merck KGaA, Ph. Eur.), Eu_2O_3 (Treibacher Industrie AG, 99.99%) and $MnC_2O_4{\cdot}2H_2O$ (Dr Paul Lohmann, chem. pure) were weighed in stoichiometric amounts. 1 wt% H_3BO_3 (Merck KGaA, Ph. Eur.) was added as a flux. Subsequently, the educts were ground in acetone in an agate mortar. After drying at ambient temperature, the obtained powder blends were heated at 1000 °C for 2 h in air to decompose the carbonates. Afterwards the samples were ground and finally calcined in alumina boats at 1200 °C for 12 h in reducing forming gas flow (Westfalen, 5% H_2, 95% N_2). After calcination, hard sinter bodies with a slightly yellow body colour were obtained which were subsequently ground to a fine powder.

Characterization

Phase purity was investigated using X-ray powder diffractometry (XRD). XRD patterns were recorded on a Rigaku MiniFlex II diffractometer working in Bragg–Brentano geometry using Cu K_α radiation. Step width and integration time were 0.02 and 1 s, respectively.

PL spectra and photoluminescence excitation (PLE) spectra were recorded on an Edinburgh Instruments FSL900 spectrometer equipped with a Xe arc lamp (450 W) and a cooled (−20 °C) single-photon counting photomultiplier (Hamamatsu R2658P). PL spectra were corrected by using a correction file obtained from a tungsten incandescent lamp certified by the National Physical Laboratory, UK.

For photoluminescence decay (PLD) measurements on Eu^{2+}, the spectrometer was equipped with a picosecond pulsed laser (5 mW, pulse width = 76.6 ps, λ_{em} = 375 nm). For PLD measurements on Mn^{2+} a microsecond pulsed Xe lamp (100 W, pulse width = 1 μs) was attached to the spectrometer.

For temperature dependent measurements the spectrometer was equipped with a cryostat (Oxford Instruments). Liquid nitrogen was used as a cooling agent. Temperature stabilization time was 60 s and tolerance was set to ±3 K.

Diffuse reflectance (DR) spectra were recorded on an Edinburgh Instruments FS900 spectrometer equipped with a Xe arc lamp (450 W), a cooled (−20 °C) single-photon counting photomultiplier (Hamamatsu R928) as well as a Teflon-coated integration sphere. $BaSO_4$ (99.998%, Sigma-Aldrich) was used as a reflectance standard.

External quantum efficiencies η_{ext} were determined using the approach of Kawamura *et al.*[14] To this end, PL spectra of the sample as well as of the excitation source were recorded in the integration sphere. From this, η_{ext} can be calculated by the following equation:

$$\eta_{ext} = \frac{\int I_{em}(\lambda)\mathrm{d}\lambda}{\int I_{ex}(\lambda)\mathrm{d}\lambda - \int I'_{ex}(\lambda)\mathrm{d}\lambda} \quad (1)$$

where $I_{em}(\lambda)$ is the emission intensity of the sample. $I_{ex}(\lambda)$ and $I'_{ex}(\lambda)$ are the intensities of the excitation source in the absence and presence of the sample.

3. Results and discussion

Collected XRD patterns of doped and also of undoped $BaCa_2Si_3O_9$ samples as well as the ICDD reference cards of $BaCa_2Si3O_9$ and SiO_2 are presented in Fig. 1. The XRD patterns indicate the formation of the triclinic $BaCa_2Si_3O_9$ phase. Furthermore, with increasing doping concentrations of Eu^{2+} and Mn^{2+}, no change in the host structure can be observed. However, samples with $x > 0.1$ show an additional reflex at about 25.9° which can be assigned to SiO_2. This proves the successful synthesis of the investigated $BaCa_2Si_3O_9$:Eu^{2+},Mn^{2+} phosphors with a Mn^{2+} concentration up to $x = 0.1$.

Fig. 2 shows DR spectra of undoped $BaCa_2Si_3O_9$ host material and also of $Ba_{0.99}Eu_{0.01}Ca_2Si_3O_9$ and $Ba(Ca_{0.95}Mn_{0.05})_2Si_3O_9$. Undoped $BaCa_2Si_3O_9$ exhibits high reflectance between 250 and 800 nm. Thus, undoped $BaCa_2Si_3O_9$ possess a white body colour. The DR spectrum of $Ba_{0.99}Eu_{0.01}Ca_2Si_3O_9$ shows a broad absorption band between 250 and 450 nm due to the allowed $[Xe]4f^7$–$[Xe]4f^6 5d^1$-transition of Eu^{2+}. Because of the absorption band in the blue range of the electromagnetic spectrum, $Ba_{0.99}Eu_{0.01}Si_3O_9$ exhibits a slightly yellow body colour. The DR spectrum of $Ba(Ca_{0.95}Mn_{0.05})_2Si_3O_9$ shows absorption in the UV region between 250 and 350 nm which can be tentatively assigned to a Mn^{2+} charge transfer transition.[15]

The PLE spectrum as well as the PL spectrum of $Ba_{0.99}Eu_{0.01}Ca_2Si_3O_9$ is depicted in Fig. 3a. The PLE spectrum was recorded monitoring the 460 nm emission of Eu^{2+} and exhibits a broad band consisting of various unresolved bands.

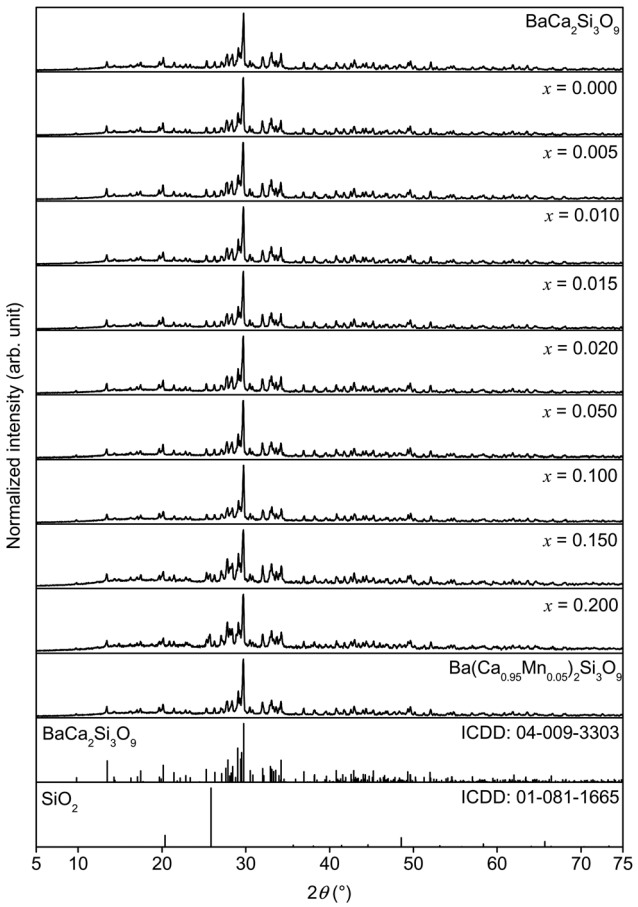

Fig. 1 XRD patterns of pure $BaCa_2Si_3O_9$ as well as of $Ba_{0.99}Eu_{0.01}(Ca_{1-x}Mn_x)_2Si_3O_9$ and $Ba(Ca_{0.95}Mn_{0.05})_2Si_3O_9$.

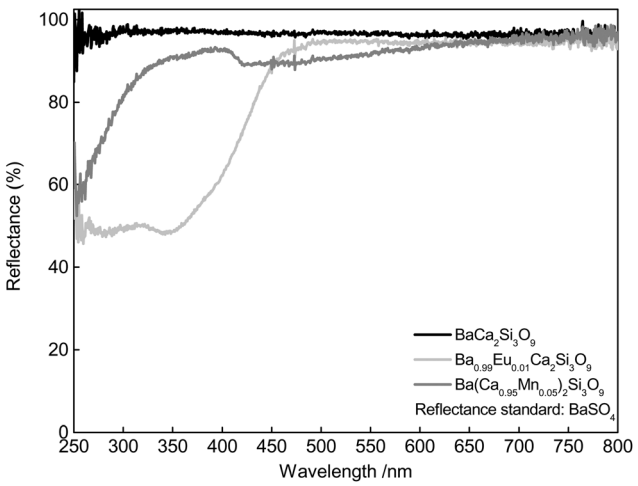

Fig. 2 DR spectra of pure $BaCa_2Si_3O_9$ as well as of $Ba_{0.99}Eu_{0.01}Ca_2Si_3O_9$ and $Ba(Ca_{0.95}Mn_{0.05})_2Si_3O_9$.

This band is due to excitation from the $[Xe]4f^7$ ground state to the $[Xe]5d^1$ multiplet of Eu^{2+}. The PL spectrum of $Ba_{0.99}Eu_{0.01}Ca_2Si_3O_9$ (λ_{ex} = 320 nm) shows an emission band

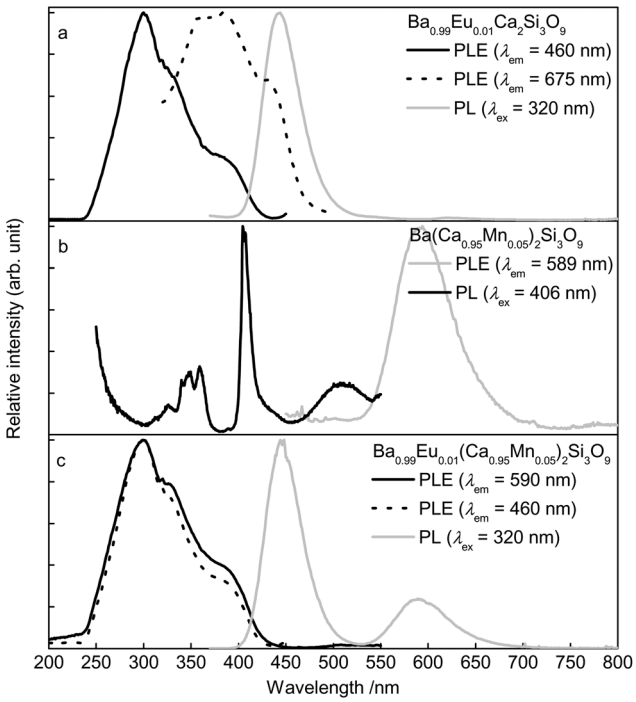

Fig. 3 Room temperature PLE and PL spectra of $Ba_{0.99}Eu_{0.01}Ca_2Si_3O_9$ (a), $Ba(Ca_{0.95}Mn_{0.05})_2Si_3O_9$ (b), and $Ba_{0.99}Eu_{0.01}(Ca_{0.95}Mn_{0.05})_2Si_3O_9$ (c).

peaking at about 444 nm with FWHM of 47 nm (2333 cm^{-1}). This emission originates from relaxation of the excited $[Xe]5d^1$ state to the $[Xe]4f^7$ ground state. Further, $Ba_{0.99}Eu_{0.01}Ca_2Si_3O_9$ possesses an emission band in the red region of the spectrum. The PLE spectrum of this emission is shown as a dotted line. Fig. 3b illustrates the PLE and PL spectra of $Ba(Ca_{0.95}Mn_{0.05})_2Si_3O_9$. Monitoring the 590 nm emission of Mn^{2+}, the PLE spectrum of $Ba(Ca_{0.95}Mn_{0.05})_2Si_3O_9$ shows various bands centred at 326, 348, 359, 405, 432, and 510 nm. These peaks can be assigned to transitions from the $^6A_1(^6S)$ ground state to $^4T_1(^4P)$, $^4E(^4D)$, $^4T_2(^4D)$, $[^4E(^4G)^4A_1(^4G)]$, $^4T_2(^4G)$, and $^4T_1(^4G)$, respectively. The PL spectrum of $Ba(Ca_{0.95}Mn_{0.05})_2Si_3O_9$ was recorded under an excitation wavelength of λ_{ex} = 405 nm and exhibits a broad band with a maximum at about 594 nm resulting from a transition from the $^4T_1(^4G)$ excited state to the $^6A_1(^6S)$ ground state. This observation is in accordance with the results given by Gaft *et al.* regarding Mn^{2+} emission in natural walstromite.[12] In addition, the Mn^{2+} emission band comprises a tailing to the red range of the visible spectrum indicating emission from different crystallographic sites. PLE as well as PL spectra of co-doped $Ba_{0.99}Eu_{0.01}(Ca_{0.95}Mn_{0.05})_2Si_3O_9$ are depicted in Fig. 3c. The PL spectrum of $Ba_{0.99}Eu_{0.01}(Ca_{0.95}Mn_{0.05})_2Si_3O_9$ shows two bands peaking at about 445 and 590 nm which can be assigned to electronic transitions of Eu^{2+} ($[Xe]5d^1$ to $[Xe]4f^7$) and Mn^{2+} ($^4T_1(^4G)$ to $^6A_1(^6S)$), respectively. PLE spectra of $Ba_{0.99}Eu_{0.01}(Ca_{0.95}Mn_{0.05})_2Si_3O_9$ were recorded, monitoring the 460 nm emission of Eu^{2+} as well as the 590 nm emission of Mn^{2+}. These PLE spectra appear similar to the PLE of singly

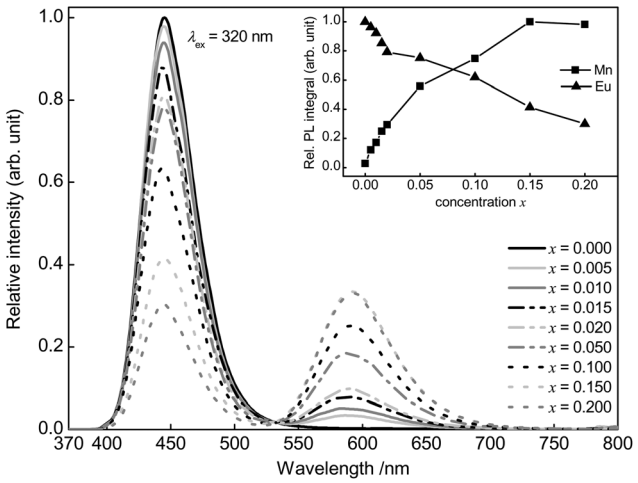

Fig. 4 PL spectra of $Ba_{0.99}Eu_{0.01}(Ca_{1-x}Mn_x)_2Si_3O_9$ and integrated PL intensity in dependence of the Eu^{2+} and Mn^{2+} concentration (inset).

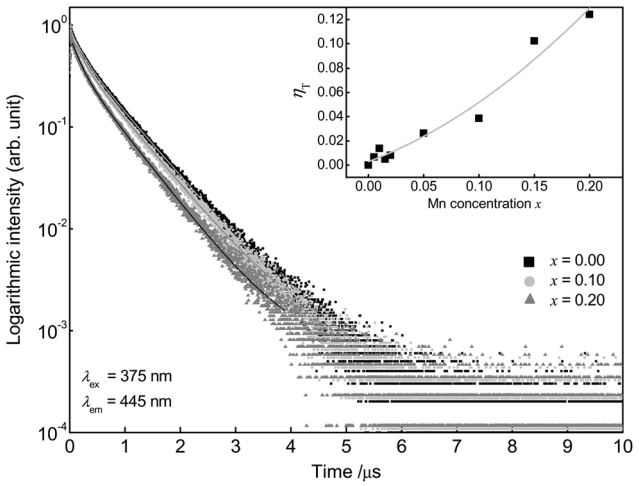

Fig. 5 PLD curves of $Ba_{0.99}Eu_{0.01}(Ca_{1-x}Mn_x)_2Si_3O_9$ and ET efficiency η_T in dependence of the Mn^{2+} concentration (inset).

doped $Ba_{0.99}Eu_{0.01}Ca_2Si_3O_9$ monitoring the blue emission of Eu^{2+}. This observation strongly implies the occurrence of ET from Eu^{2+} to Mn^{2+}.

Fig. 4 illustrates the PL spectra of the synthesized $Ba_{0.99}Eu_{0.01}(Ca_{1-x}Mn_x)_2Si_3O_9$ series with x = 0, 0.005, 0.010, 0.015, 0.020, 0.050, 0.100, 0.150, and 0.200. As can be concluded from the spectra, with increasing Mn^{2+} concentration the PL intensity of Eu^{2+} decreases. This behaviour reflects the assumption provided above regarding ET from Eu^{2+} to Mn^{2+}. The inset in Fig. 4 depicts the relative PL intensities of Eu^{2+} and Mn^{2+}. It was found that the PL intensity of Mn^{2+} increases continuously up to a Mn^{2+} concentration of x = 0.15 where a saturation effect begins. Concentration quenching of the Mn^{2+} emission was not observed for the synthesized samples.

Furthermore, PLD measurements were performed monitoring the Eu^{2+} emission to investigate the ET from Eu^{2+} to Mn^{2+} in more detail. Fluorescence lifetimes τ of $Ba_{0.99}Eu_{0.01}(Ca_{1-x}Mn_x)_2Si_3O_9$ samples with increasing Mn^{2+} content were determined, monitoring the 445 nm emission of Eu^{2+} under an excitation wavelength of λ_{ex} = 375 nm. Fig. 5 illustrates the obtained PLD curves. The PLD curves can be best fitted with a bi-exponential function applying the following equation:

$$I = A_1 e^{\frac{-t}{\tau_1}} + A_2 e^{\frac{-t}{\tau_2}} \quad (2)$$

Here, I is the luminescence intensity, A_1 and A_2 are parameters and t is the time. The terms τ_1 and τ_2 are the partial lifetimes for the exponential components. The bi-exponential shape of the PLD curves originates from two different emitting centres and suggests Eu^{2+} emission from two distinct crystallographic sites. This is thoroughly possible since $BaCa_2Si_3O_9$ provides two different Ca sites and one Ba site, as mentioned above. This assumption is backed by PLD measurements monitoring the emission at 415 and 495 nm which yield different luminescence lifetimes (τ at 415 nm = 602 ns, τ at 415 nm = 702 ns) (Fig. S1 in the ESI†). The average luminescence lifetimes τ of Eu^{2+} in $BaCa_2(Si_3O_9)$:Eu^{2+},Mn^{2+} can be derived using the above mentioned parameters and the following equation:

$$\tau = \frac{A_1\tau_1^2 + A_2\tau_2^2}{A_1\tau_1 + A_2\tau_2} \quad (3)$$

Emission fractions $frac_1$ and $frac_2$, partial lifetimes τ_1, and τ_2 and also the calculated average lifetimes are summarized in Table 1. The results show a decreasing lifetime τ of Eu^{2+} with increasing Mn^{2+} concentration. Since ET processes are usually faster than radiative transitions, this circumstance clearly indicates the occurrence of an ET from Eu^{2+} to Mn^{2+}. The ET efficiency η_T be calculated using following equation:[16]

$$\eta_T = 1 - \frac{\tau_S}{\tau_{S0}} \quad (4)$$

In this equation τ_S and τ_{S0} are the average lifetimes of Eu^{2+} in the presence and absence of Mn^{2+}. The inset of Fig. 5 illustrates the calculated values for η_T for the investigated $BaCa_2Si_3O_9$:Eu^{2+},Mn^{2+} samples as a function of the Mn^{2+} content. This shows that the ET efficiency η_T continuously

Table 1 Fluorescence lifetimes τ as well as partial lifetimes τ_1 and τ_2 and the emission fractions $frac_1$ and $frac_2$ of Eu^{2+} in $Ba_{0.99}Eu_{0.01}(Ca_{1-x}Mn_x)_2Si_3O_9$

Sample (x)	$frac_1$ (%)	τ_1 (ns)	$frac_2$ (%)	τ_2 (ns)	τ (ns)
0.000	13	212	87	698	634
0.005	14	208	86	697	629
0.010	13	206	87	690	625
0.015	13	206	87	693	630
0.020	12	204	88	687	628
0.050	13	201	87	680	617
0.100	13	193	87	673	609
0.150	15	175	85	636	569
0.200	16	176	84	629	555

increases with increasing Mn^{2+} content. For the highest Mn^{2+} concentration with $x = 0.20$, η_T amounts to 12% whereas the PL intensity of Eu^{2+} decreases around 70%. Due to faster competitive ET processes, *e.g.* migration to defect sites, a significant amount of emission energy is lost before it can be transferred to the Mn^{2+} ions. This behaviour increases with increasing Mn^{2+} concentration.

The average distance between Eu^{2+} and Mn^{2+} (R_{Eu-Mn}) in the host material at which ET occurs can be estimated by applying the following formula published by Blasse:[17]

$$R_{Ce-Mn} = 2\left[\frac{3V}{4\pi xN}\right]^{\frac{1}{3}} \quad (5)$$

Here, V is the volume of the unit cell, x the concentration of Eu^{2+} and Mn^{2+} in the host, and N is the number of available sites for the dopants in the unit cell. For $BaCa_2Si_3O_9$, V and N are 396.01 Å^3 and 6, respectively. Using this equation for x = 0.005, 0.010, 0.015, 0.020, 0.050, 0.100, 0.150, and 0.200, (R_{Eu-Mn}) is calculated to be 20.3, 18.5, 17.1, 16.1, 12.8, 10.5, 9.2, and also 8.4 Å, respectively. The Mn^{2+} concentration where the Eu^{2+} PL intensity is one-half of that in the sample without Mn^{2+} is called critical concentration x_c. Plugging in x_c into formula (5), the critical distance R_c can be derived. R_c is defined as the distance where the probability of ET from sensitizer to activator equals the probability of radiative transition in the sensitizer. For $Ba_{0.99}Eu_{0.01}(Ca_{1-x}Mn_x)_2Si_3O_9$, x_c was determined to be 0.134. From this, R_c is calculated to be 9.6 Å.

To elucidate the characteristics of the ET process in $Ba_{0.99}Eu_{0.01}(Ca_{1-x}Mn_x)_2Si_3O_9$, the obtained decay curves were analysed by applying the Inokuti–Hirayama model. Assuming a uniform distribution of Eu^{2+} and Mn^{2+} in the host structure, and neglecting further energy migration processes besides the ET from Eu^{2+} to Mn^{2+}, the time-dependent course of the PL intensity of Eu^{2+} can be described by following equation:[18]

$$I(t) = I_0 \times e^{-\frac{t}{\tau_0} - \alpha\left(\frac{t}{\tau_0}\right)^{\frac{3}{S}}} \quad (6)$$

In this equation, t is the time, $I(t)$ is the PL intensity after excitation, I_0 is the PL intensity at $t = 0$, τ_0 is the intrinsic luminescence lifetime of the sensitizer in the absence of the activator, α is a parameter for the probability of ET. S is related to the electronic multipole character of the ET. S = 6, 8, and 10 corresponds to dipole–dipole, dipole–quadrupole, and quadrupole–quadrupole interactions, respectively. Modifying eqn (6) leads to following relation:

$$\ln\left[-\ln\left(\frac{I(t)}{I_0}\right) - \left(\frac{t}{\tau_0}\right)\right] \sim \ln\left(\frac{t}{\tau_0}\right)^3 \quad (7)$$

Plotting the PLD curves using this relation yields a straight line with a slope equal to 1/S. The obtained curves for the measured $Ba_{0.99}Eu_{0.01}(Ca_{1-x}Mn_x)_2Si_3O_9$ samples with x = 0.005, 0.010, 0.015, 0.020, 0.050, 0.100, 0.150, and 0.200 are depicted in Fig. 6. The calculated S values are roughly coincident with the theoretical value of S = 8. This result suggests

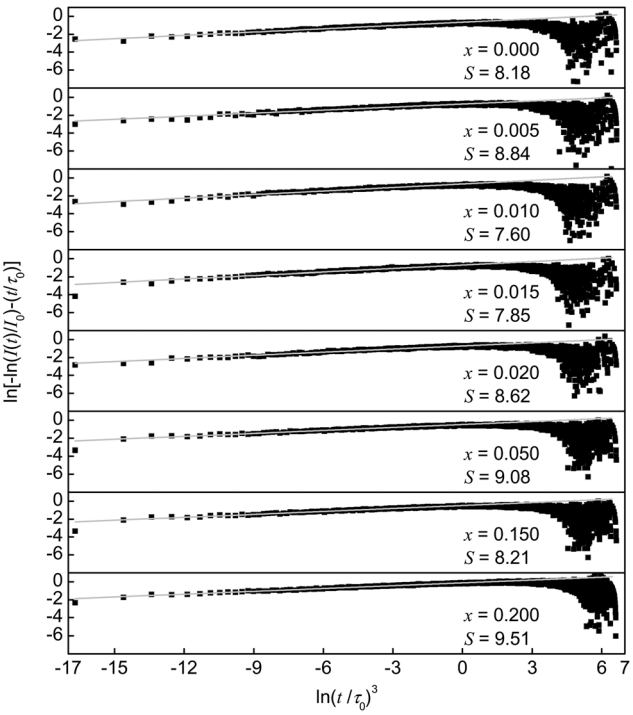

Fig. 6 Plots of ln[−ln(I(t)/I_0) − (t/τ_0)] *versus* ln(t/τ_0)^3. Experimental data are represented by the dots. Grey lines represent the fitting functions.

dipole–quadrupole interactions as the dominant mechanism of ET from Eu^{2+} to Mn^{2+} in co-doped $BaCa_2Si_3O_9$:Eu^{2+},Mn^{2+}.

This finding is quite reasonable since the electronic [Xe]4f^7–[Xe]4f^{6}5d^1-transition in Eu^{2+} is allowed whereas the electronic [Ar]3d^5–[Ar]3d^5-transition in Mn^{2+} is forbidden. Therefore, the critical distance R_c for ET from Eu^{2+} to Mn^{2+} can be calculated using the spectral overlap method:[17,19]

$$R_c{}^8 = 0.63 \times 10^{28}\,\frac{f_q\lambda_S{}^2Q_A}{f_dE^4}\int F_S(E)F_A(E)dE \quad (8)$$

In this formula $f_q = 10^{-10}$ and $f_d = 10^{-7}$ are the oscillator strengths of dipole and quadrupole electronic absorption transitions, respectively, for Mn^{2+}. The absorption cross section Q_A of Mn^{2+} can be expressed using the relationship $Q_A = 4.8 \times 10^{-16}f_d$ derived by Blasse. λ_S is the emission wavelength of Eu^{2+}. E is the energy of maximal spectral overlap. From this, the critical distance R_c is calculated to be 8.9 Å. This value is in accordance with the one calculated using Blasse's approach (9.6 Å).

To investigate the temperature dependence of the PL of co-doped $Ba_{0.99}Eu_{0.01}(Ca_{0.90}Mn_{0.10})_2Si_3O_9$, PL spectra were recorded from 100 to 800 K. The obtained PL spectra are depicted in Fig. 7. The spectra demonstrate that with increasing temperature PL intensity of Eu^{2+} and Mn^{2+} decreases due to thermal quenching. The inset of Fig. 7 illustrates the normalized PL integrals *versus* their temperature. From this, activation energy E_A for thermal quenching can generally be

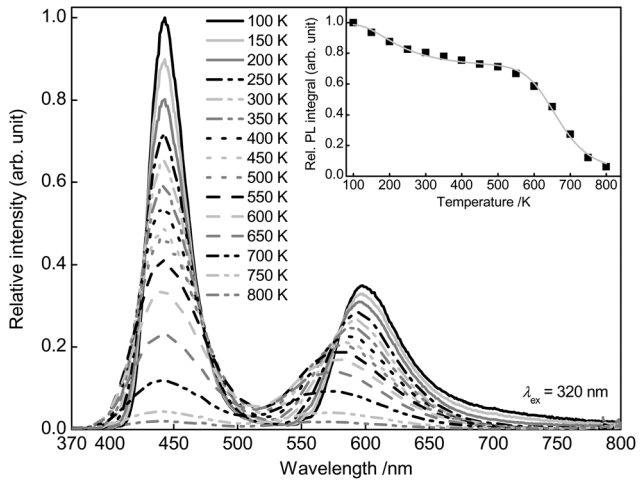

Fig. 7 PL spectra of $Ba_{0.99}Eu_{0.01}(Ca_{0.90}Mn_{0.10})_2Si_3O_9$ from 100 to 800 K and PL integral in dependence of the temperature (inset).

estimated by fitting the data points by a Fermi–Dirac distribution:

$$I(T) = \frac{I_0}{1 + B \times e^{\frac{-E_A}{kT}}} \quad (9)$$

In this equation, $I(T)$ is the luminescence intensity at a certain temperature and I_0 is the luminescence intensity at zero Kelvin. B is the quenching frequency factor, T is the temperature and k is the Boltzmann constant. However, due to an additional turning point, the present data points cannot be fitted by ordinary Fermi–Dirac distribution. Therefore, eqn (9) is expanded to a sum of two weighed Fermi–Dirac distributions:

$$I(T) = A \frac{I_{0,a}}{1 + B \times e^{\frac{-E_{A,a}}{kT}}} + (1 - A) \frac{I_{0,b}}{1 + B \times e^{\frac{-E_{A,b}}{kT}}} \quad (10)$$

Here, $I_{0,a}$ and $I_{0,b}$ are the PL intensities at zero Kelvin. A describes the fraction of the first term. From this, $E_{A,a}$ and $E_{A,b}$ were determined to be about 0.07 and 0.84 eV, respectively. Plugging in the values for $E_{A,a}$ and $E_{A,b}$ in eqn (11) yields $T_{1/2,a}$ and $T_{1/2,b}$:

$$T_{1/2} = \frac{-E_A}{k \times \ln\left(\frac{1}{B}\right)} \quad (11)$$

$T_{1/2}$ is the temperature at which PL intensity of a luminescent centre is decreased to one-half of its maximum. For $Ba_{0.99}Eu_{0.01}(Ca_{0.90}Mn_{0.10})_2Si_3O_9$, $T_{1/2,a}$ and $T_{1/2,b}$ were calculated to be 242 and 666 K, respectively. The PL intensities originating from Eu^{2+} and Mn^{2+} were plotted separately (Fig. S2 and S3 in the ESI†). From that it can be seen that the bi-sigmoidal temperature behaviour strongly decreases if investigating the PL intensities of Eu^{2+} solely. Due to overlapping of the red emission band the bi-sigmoidal shape does not vanish completely. To examine the origin of this double sigmoidal quenching behaviour, PL of singly doped $Ba_{0.99}Eu_{0.01}Si_3O_9$ was measured in the temperature range from 100 to 800 K as well (Fig. S4 in the ESI†). At low temperatures an additional emission band extending from about 600 to 750 nm arises. PLD measurements of this emission band revealed a fluorescence lifetime of about 945 ns (Fig. S5 in the ESI†). This value matches well with the decay time of Eu^{2+}. Furthermore, the obtained PLD curve shows mono-exponential decay behaviour, indicating emission from one particular crystallographic site. These Eu^{2+} ions presumably occupy the 6-fold coordinated Ca2 sites in $BaCa_2Si_3O_9$. On this small site, the crystal field splitting of the d-orbitals of Eu^{2+} is rather high because of which the lower edge of the [Xe]5d multiplet is moved towards the ground state. Due to relatively low emission energies in the red spectral range and consequently strong multi-phonon relaxation as well as large Stokes shift, this emission exhibits a lower quenching temperature. Furthermore, with increasing temperature a blue shift of Mn^{2+} emission can be observed. This behaviour is due to an increasing average distance between the Mn^{2+} ions and their oxygen ligands with increasing temperatures. As a consequence, the crystal field splitting of the 3d orbitals of Mn^{2+} decreases resulting in a shift of the $^4T_1(^4G) \rightarrow {}^6A_1(^6S)$ transition to higher energies.[20]

To obtain more detailed information regarding the temperature dependent behaviour of $Ba_{0.99}Eu_{0.01}(Ca_{0.90}Mn_{0.10})_2Si_3O_9$, PLD measurements were performed from 100 to 500 K. Fig. 8 depicts the PLD curves of $Ba_{0.99}Eu_{0.01}(Ca_{0.90}Mn_{0.10})_2Si_3O_9$ monitoring the 445 nm emission of Eu^{2+}. The curves can be best fitted with a bi-exponential function, suggesting Eu^{2+} emission from two distinct crystallographic sites as mentioned previously. The derived fluorescence lifetimes are presented in Table 2 and show an unusual increase with increasing temperatures. This phenomenon was only reported by a few authors and is still uncommon.[21,22] According to Meijerink and Blasse, this behaviour is presumably caused by thermal population of

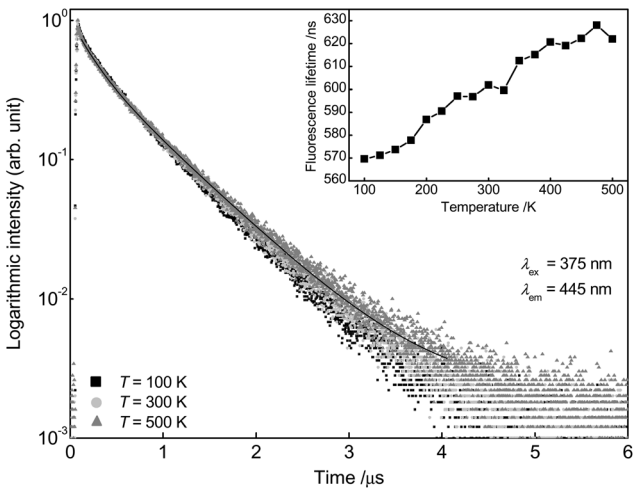

Fig. 8 PLD curves of $Ba_{0.99}Eu_{0.01}(Ca_{0.90}Mn_{0.10})_2Si_3O_9$ at 100, 300 and 500 K monitoring the emission of Eu^{2+}. Fluorescence lifetimes in dependency of temperature (inset).

Table 2 Fluorescence lifetimes τ as well as partial lifetimes τ_1 and τ_2, and the emission fractions $frac_1$ and $frac_2$ of Eu^{2+} and Mn^{2+} in $Ba_{0.99}Eu_{0.01}(Ca_{1-x}Mn_x)_2Si_3O_9$ from 100 to 500 K

	Eu^{2+}					Mn^{2+}				
T (K)	$frac_1$ (%)	τ_1 (ns)	$frac_2$ (%)	τ_2 (ns)	τ (ns)	$frac_1$ (%)	τ_1 (ms)	$frac_2$ (%)	τ_2 (ms)	τ (ms)
100	16	214	84	637	570	9	19	91	47	44
125	15	205	85	637	571					
150	14	190	86	635	574	9	17	91	45	42
175	13	191	87	638	578					
200	12	184	88	644	587	6	13	94	41	39
225	12	190	88	645	591					
250	13	205	87	656	597	8	15	92	38	36
275	13	199	87	656	597					
300	12	199	88	659	602	10	16	90	35	33
325	13	187	87	663	600					
350	15	215	85	681	612	5	10	96	31	30
375	15	216	85	684	615					
400	14	216	86	687	621	8	12	92	29	28
425	14	195	86	689	619					
450	13	199	87	688	622	4	7	96	26	26
475	15	211	85	701	628					
500	13	201	87	687	622	4	7	96	24	24

higher energetic 4f ^{6}5d states. Excited states in Eu^{2+} can either be (spin) octets or sextets. The sextet states are at higher energies than the octet states according to Hund's rule. With increasing temperature the higher energetic sextet states will be populated. For these states, transition to the $^8S_{7/2}$ ground state is spin-forbidden resulting in lower decay rates and thus longer fluorescence lifetimes.[22] Fluorescence lifetimes of Mn^{2+} emission in dependency of temperature were measured, too. The obtained PLD curves are depicted in Fig. 9 and can be well fitted with a bi-exponential function. This result is consistent with the assumption made above that Mn^{2+} is located on two different crystallographic sites. The calculated average lifetimes of Mn^{2+} are summarized in Table 2. With increasing temperature, Mn^{2+} fluorescence lifetimes decrease continuously due to an increase in non-radiative relaxation to the ground state. Therefore, it can be concluded that thermal quenching of emission in $BaCa_2Si_3O_9$:Eu^{2+},Mn^{2+} is primarily caused by Mn^{2+} ions. As deduced from PLD curves of Mn^{2+} emission as well as from ionic radii of Ba^{2+}, Ca^{2+} and Mn^{2+}, it can be concluded that Mn^{2+} ions preferably occupy the two Ca sites in $BaCa_2Si_3O_9$. Since the ionic radii of 6- and 8-fold coordinated Mn^{2+} are smaller compared to those of Ca^{2+}, the excited states of Mn^{2+} can strongly be polarized. This leads to an increase in the equilibrium distance between Mn^{2+} and its oxygen ligands and therefore to a shift of the ground and excited state parabolas in the configurational coordinate diagram. Further, the crossing point of the parabolas is shifted to lower energy, and thus to a lower activation energy for thermal quenching.

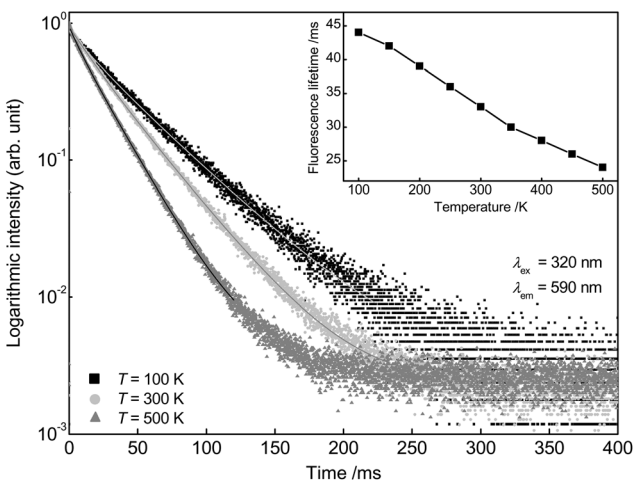

Fig. 9 PLD curves of $Ba_{0.99}Eu_{0.01}(Ca_{0.90}Mn_{0.10})_2Si_3O_9$ at 100, 300 and 500 K monitoring the emission of Mn^{2+}. Fluorescence lifetimes in dependency of temperature (inset).

To investigate the PL efficiency of the $Ba_{0.99}Eu_{0.01}$-$(Ca_{1-x}Mn_x)_2Si_3O_9$ samples, external quantum efficiencies η_{ext} were measured as mentioned above. To the best of our understanding, external quantum efficiency η_{ext} is defined as:

$$\eta_{ext} = \frac{N_{emission}}{N_{absorption}} \quad (12)$$

where $N_{emission}$ is the number of photons emitted by the phosphor and $N_{absorption}$ is the number of photons absorbed by the phosphor. The resulting quantum efficiencies η_{ext} are summarized in Table 3. For the investigated samples η_{ext} is around 30%. The low quantum efficiency of $BaCa_2Si_3O_9$:Eu^{2+},Mn^{2+} can be ascribed to the overlap of the blue emission band and the excitation band of the red emission of Eu^{2+}. Due to ET from the blue Eu^{2+} site to the red Eu^{2+} site which is thermally quenched, η_{ext} decreases.

According to the relevant PL spectra, Commission International de l'Eclairage 1931 (CIE) chromaticity coordinates were calculated. Fig. 10 depicts the CIE chromaticity diagram

Table 3 External quantum efficiencies η_{ext} and CIE colour coordinates of $Ba_{0.99}Eu_{0.01}(Ca_{1-x}Mn_x)_2Si_3O_9$

Sample	η_{ext}	CIE (x|y)
x = 0.000	0.31	(0.151|0.043)
x = 0.005	0.31	(0.163|0.053)
x = 0.010	0.30	(0.170|0.060)
x = 0.015	0.31	(0.182|0.073)
x = 0.020	0.32	(0.190|0.080)
x = 0.050	0.34	(0.224|0.112)
x = 0.100	0.36	(0.260|0.146)
x = 0.150	0.26	(0.323|0.210)
x = 0.200	0.30	(0.354|0.240)

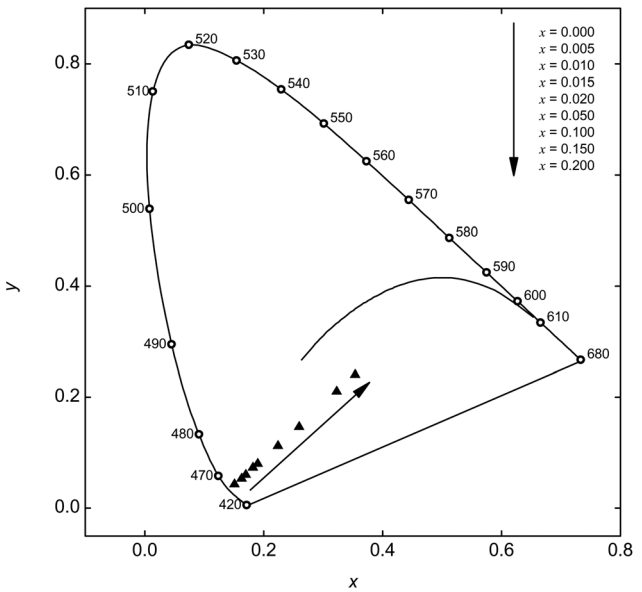

Fig. 10 CIE chromaticity diagram of $Ba_{0.99}Eu_{0.01}(Ca_{1-x}Mn_x)_2Si_3O_9$ with different Mn^{2+} concentrations.

for $Ba_{0.99}Eu_{0.01}(Ca_{1-x}Mn_x)_2Si_3O_9$ with x = 0, 0.005, 0.010, 0.015, 0.020, 0.050, 0.100, 0.150, and 0.200. By increasing the Mn^{2+} concentration, the chromaticity coordinates can be shifted from blue to magenta colour tones. Due to the lack of emission in the green spectral range, $BaCa_2Si_3O_9:Eu^{2+},Mn^{2+}$ has to be combined with an additional green emitting phosphor to generate white light, such as $(Ba,Sr)_2SiO_4:Eu^{2+}$, $Sr_{12}Al_{14}O_{32}Cl_2:Eu^{2+}$ or $KBaBP_2O_8:Tb^{3+}$.[23] Fig. S6† shows a simulated white emission spectrum consisting of $Ba_{0.99}Eu_{0.01}Ca_{(0.80}Mn_{0.20)_2}Si_3O_9$ and $(Ba_{0.49}Sr_{0.49}Eu_{0.02})_2SiO_4$. The CIE 1931 colour coordinates of the spectrum are x = 0.327 and y = 0.333 which result in a correlated colour temperature (CCT) of 5745 K. The colour rendering index (CRI) R_a of the simulated spectrum is equal to 82. This CCT is similar to that of a phosphor-converted white LED consisting of a blue LED chip and $YAG:Ce^{3+}$ (CCT = 5600 K) whereas the CRI is higher compared to that of this phosphor-converted LED (R_a = 71).[24]

4. Conclusions

A series of $BaCa_2Si_3O_9:Eu^{2+},Mn^{2+}$ powder samples with various Mn^{2+} concentrations was prepared *via* high temperature solid state synthesis. Excited by UV radiation, $BaCa_2Si_3O_9:Eu^{2+},Mn^{2+}$ shows two emission bands located at about 444 and 594 nm originating from Eu^{2+} and Mn^{2+}, respectively. It turned out that Eu^{2+} ions in $BaCa_2Si_3O_9:Eu^{2+},Mn^{2+}$ occupy the 8-fold coordinated Ba and Ca1 sites as well as the 6-fold coordinated Ca2 sites. Mn^{2+} ions tend to occupy both Ca sites. These results are confirmed by PLD measurements. The highest PL intensity of Mn^{2+} was found at a Mn^{2+} concentration of x = 0.15. It was further demonstrated that ET from Eu^{2+} to Mn^{2+} in $BaCa_2Si_3O_9:Eu^{2+},Mn^{2+}$ is of resonant type and occurs *via* dipole–quadrupole interaction. The critical distance R_c between Eu^{2+} and Mn^{2+} was derived by using Blasse's concentration quenching method as well as the spectral overlap method and was calculated to be 9.6 and 8.9 Å, respectively. Temperature dependent PL measurements prove a "double" sigmoidal decrease of the PL intensity of Eu^{2+}. Therefore, $BaCa_2Si_3O_9:Eu^{2+},Mn^{2+}$ has two $T_{1/2}$ values, $T_{1/2,a}$ and $T_{1/2,b}$, which were calculated to be 242 and 666 K, respectively. In addition to that, PLD measurements revealed an unusual increase of Eu^{2+} fluorescence lifetime, which presumably originates from thermal population of higher excited energy levels. Temperature dependent PLD measurements on the Mn^{2+} emission suggest that thermal quenching in $BaCa_2Si_3O_9:Eu^{2+},Mn^{2+}$ is primarily caused by Mn^{2+} ions. CIE 1931 colour points can be tuned from the blue to the magenta colour range.

Acknowledgements

The authors are grateful to Merck KGaA Darmstadt, Germany, for generous financial support.

Notes and references

1 S. Nakamura, P. Stephen and F. Gerhard, *The Blue Laser Diode: The Complete Story*, Springer-Verlag, Berlin/Heidelberg, 1997.
2 (*a*) C. Feldmann, T. Jüstel, C. R. Ronda and P. J. Schmidt, *Adv. Funct. Mater.*, 2003, **13**, 511–516; (*b*) E. F. Schubert and J. K. Kim, *Science*, 2005, **308**, 1274–1278.
3 H. S. Jang, W. B. Im, D. C. Lee, D. Y. Jeon and S. S. Kim, *J. Lumin.*, 2007, **126**, 371–377.
4 Y. Uchida and T. Taguchi, *Opt. Eng.*, 2005, **44**, 124003.
5 M. Shang, C. Li and J. Lin, *Chem. Soc. Rev.*, 2014, **43**, 1372.
6 (*a*) W. Lv, M. Jiao, Q. Zhao, B. Shao, W. Lü and H. You, *Inorg. Chem.*, 2014, **53**, 11007–11014; (*b*) W.-J. Yang and T.-M. Chen, *Appl. Phys. Lett.*, 2006, **88**, 101903.
7 P. Eskola, *Am. J. Sci.*, 1922, **4**, 331–375.
8 J. T. Alfors, M. C. Stinson and R. A. Matthews, *Am. Mineral.*, 1965, **50**, 314–340.

9 L. S. Dent Glasser and F. P. Glasser, *Am. Mineral.*, 1968, **53**, 9–13.
10 M. C. Barkley, R. T. Downs and H. Yang, *Am. Mineral.*, 2011, **96**, 797–801.
11 S. Yao, L. Xue and Y. Yan, *Opt. Laser Technol.*, 2011, **43**, 1282–1285.
12 M. Gaft, H. Yeates and L. Nagli, *Eur. J. Mineral.*, 2013, **25**, 71–77.
13 R. D. Shannon, *Acta Crystallogr., Sect. A: Cryst. Phys., Diffr., Theor. Gen. Cryst.*, 1976, **32**, 751–767.
14 Y. Kawamura, H. Sasabe and C. Adachi, *Jpn. J. Appl. Phys.*, 2004, **43**, 7729–7730.
15 (*a*) A. Mehra, *Jpn. J. Appl. Phys.*, 1968, **7**, 963–964; (*b*) E. van der Kolk, P. Dorenbos, C. W. van Eijk, A. P. Vink, M. Weil and J. P. Chaminade, *J. Appl. Phys.*, 2004, **95**, 7867.
16 (*a*) H. C. Kandpal and H. B. Tripathi, *Indian J. Pure Appl. Phys.*, 1979, **17**, 587–589; (*b*) P. Paulose, G. Jose, V. Thomas, N. Unnikrishnan and M. Warrier, *J. Phys. Chem. Solids*, 2003, **64**, 841–846.
17 G. Blasse, *Philips Res. Rep.*, 1969, **24**, 131–144.
18 M. Inokuti and F. Hirayama, *J. Chem. Phys.*, 1965, **43**, 1978.
19 D. L. Dexter, *J. Chem. Phys.*, 1953, **21**, 836.
20 Y. Tanabe and S. Sugano, *J. Phys. Soc. Jpn.*, 1954, **9**, 766–779.
21 (*a*) J. P. Spoonhower and M. S. Burberry, *J. Lumin.*, 1989, **43**, 221–226; (*b*) T. Tsuboi and P. Silfsten, *J. Phys.: Condens. Matter*, 1991, **3**, 9163–9167; (*c*) C. K. Duan, A. Meijerink, R. J. Reeves and M. F. Reid, *J. Alloys Compd.*, 2006, **408–412**, 784–787.
22 A. Meijerink and G. Blasse, *J. Lumin.*, 1990, **47**, 1–5.
23 (*a*) B. Han, J. Zhang, P. Li and H. Shi, *Phys. Status Solidi A*, 2014, **211**, 2483–2487; (*b*) Z. Jiang, Z. Sun, X. Su, L. Duan and X. Yu, *J. Alloys Compd.*, 2013, **577**, 683–686; (*c*) T. L. Barry, *J. Electrochem. Soc.*, 1968, **115**, 1181–1184.
24 M. R. Krames, O. B. Shchekin, R. Mueller-Mach, G. O. Mueller, L. Zhou, G. Harbers and M. G. Craford, *J. Disp. Technol.*, 2007, **3**, 160–175.